# Coronary Interventions

# Thrombogenicity and Early Vascular Healing Response in Metallic Biodegradable Polymer-Based and Fully Bioabsorbable Drug-Eluting Stents

Tobias Koppara, MD; Qi Cheng, MD; Kazuyuki Yahagi, MD; Hiroyoshi Mori, MD;
Oscar David Sanchez, MD; Julia Feygin, PhD; Eric Wittchow, PhD; Frank D. Kolodgie, PhD;
Renu Virmani, MD; Michael Joner, MD

***Background***—Acute thrombogenicity and re-endothelialization represent clinically relevant end points pertaining to the safety of coronary stents, which have not been compared among biodegradable polymer-based drug-eluting metallic stents and fully bioabsorbable scaffolds to date.

***Methods and Results***—We investigated comparative outcomes with respect to acute thrombogenicity and re-endothelialization among thin-strut biodegradable polymer metallic everolimus eluting stents (EES), thick-strut fully bioabsorbable EES, thick-strut biodegradable polymer metallic biolimus-eluting stents and control bare metal stents. An ex-vivo porcine arterio-venous shunt model was used to assess platelet aggregation, whereas a healthy rabbit model of iliofemoral stent implantation was used to assess re-endothelialization and inflammation. Confocal microscopy was used to detect fluorescently labeled antibody staining directed against CD61/CD42b for the identification of aggregated thrombocytes, CD14/PM-1, and RAM-11 for identification of neutrophils and monocytes/macrophages. Endothelial recovery was assessed by scanning electron microscopy, whereas CD31/PECAM-1 was used to confirm endothelial maturity. EES demonstrated significantly less acute thrombogenicity compared with bioabsorbable EES and biolimus-eluting stents. EES showed greater re-endothelialization at 28 days and reduced inflammatory cell adhesion of monocytes/macrophages at 14 days compared with bioabsorbable EES. Only bare metal stents showed complete re-endothelialization at 28 days.

***Conclusions***—These outcomes indicate differential trends in thrombogenicity and vascular healing among contemporary stents used in clinical practice and suggest a need for long-term adjunct antithrombotic pharmacotherapy for bioabsorbable EES. (***Circ Cardiovasc Interv***. 2015;8:e002427. DOI: 10.1161/CIRCINTERVENTIONS.115.002427.)

**Key Words:** coronary artery disease ■ drug delivery ■ drug-eluting stents ■ polymer

Delayed vascular healing after drug-eluting stent implantation (DES) has been shown to be an important determinant of stent thrombosis in preclinical and autopsy studies[1,2] and is a key contributing mechanism of stent failure, including restenosis.[3]

Although protective function against acute thrombogenicity has been assigned to selected 2nd generation permanent polymeric DES when compared with 1st generation DES and bare metal stents (BMS) in recent preclinical and clinical studies,[4–6] this effect has not yet been demonstrated for biodegradable polymer–based DES. Furthermore, comparative assessment of acute thrombogenicity and other major components of vascular healing, that is, endothelialization of stent struts, has not been determined for the current generation of stents and may provide valuable insights into predictable clinical performance of these devices. Novel biodegradable polymeric stent coatings and bioabsorbable stents have attracted considerable attention in contemporary clinical practice,[7–9] and it seems intuitive that different trends in stent design and composition among contemporary DES and bioabsorbable stents may affect acute thrombogenicity and vascular healing.

The current study therefore aimed to address these clinically relevant end points in established animal models. Endothelial restoration and inflammatory reaction were examined in thin-strut biodegradable polymer metallic everolimus-eluting stents (EES) against thick-strut fully bioabsorbable EES (bEES), thick-strut biodegradable polymer metallic biolimus-eluting stents (BES), and control BMS in the rabbit iliofemoral artery model, whereas acute thrombogenicity of the same devices was tested in a previously established porcine arteriovenous shunt model.[10]

## WHAT IS KNOWN

- Acute thrombogenicity and re-endothelialization represent important preclinical end points pertaining to stent safety. Stent design and geometry as well as polymer coating and drug release kinetics are well known to impact differentially on clinical performance of contemporary stents.

## WHAT THE STUDY ADDS

- This preclinical study shows biologically meaningful differences in thrombogenicity, inflammatory response, and re-endothelialization among contemporary stents used in clinical practice. The findings suggest differential concomitant antithrombotic therapy may be needed among current thin-strut metallic drug-eluting stent and thick-strut fully absorbable stents.

## Methods

The study protocol was approved by the Institutional Animal Care and Use Committee of the Medstar Research Institute and conformed to the position of the American Heart Association on use of animals in research and the Guide for the Care and Use of Laboratory Animals published by the US National Institutes of Health.[11]

## Experimental Set-Up

### Test Devices and Grouping

Four different devices were implanted. The test device was a thin-strut biodegradable polymer metallic EES (Synergy, Boston Scientific, Marlborough, MA), 3.0×16 mm, n=18 (platinum-chromium [PtCr] platform, 74 µm strut thickness, abluminally coated biodegradable PLGA copolymer, releasing everolimus), and was compared with a thick-strut fully bioabsorbable bEES (Absorb BVS, Abbott Vascular, Santa Clara, CA), 3.0×18 mm, n=18 (poly(L-lactide) [PLLA] bioabsorbable platform, 150 µm strut thickness, circumferentially coated biodegradable PDLLA polymer, releasing everolimus), and

a thick-strut biodegradable polymer metallic BES (BioMatrix Flex, Biosensors, Newport Beach, CA), 3.0×14 mm, n=18 (stainless steel platform, 120 µm strut thickness, abluminally coated biodegradable PDLLA polymer, releasing biolimus). A thin-strut BMS (Omega, Boston Scientific, Marlborough, MA), 3.0×16 mm, n=18 (PtCr platform, 81 µm strut thickness), served as control.

## Animal Models

Two different animal models were used in this study. An ex vivo arterio-venous porcine shunt model served to assess acute thrombogenicity and acute inflammatory cell adhesion (n=4 pigs), whereas endothelialization and macrophage deposition were investigated in a healthy rabbit model of iliofemoral stent implantation (n=24 animals; Figure 1).

### Porcine Ex Vivo Arterio-Venous Shunt Model

A total of 4 healthy domestic farm pigs (13–15 weeks, Thomas D. Morris Inc, Reisterstown, MD) were included in the study. A porcine ex vivo arteriovenous shunt model involving a test circuit of 3 different in-line test stents was used for a period of 55 to 60 minutes to study the extent of platelet adherence, thrombus formation, and acute inflammation in the devices as previously described.[10] Each shunt model had 3 stents and each animal had 2 shunt experiments using a total of n=6 devices per animal. Target blood–activated clotting times (ACT) between 150 s and 200 s were achieved with intravenous heparin (100 IU/kg) dosing without antiplatelet agents. Dual antiplatelet therapy was intentionally not administered in the applied animal models because we aimed to study the differential impact of stent design and stent components on platelet activation and aggregation. At the conclusion of each shunt run, stents were gravity perfused with Ringer's Lactate, fixed in 10% neutral buffered formalin, and bisected longitudinally. The experimental set up is detailed in the Data Supplement methods.

### Rabbit Model of Iliac Stent Implantation

A total of 24 healthy New Zealand White rabbits (5–6 months, Millbrook Laboratories, Amherst, MA) were included in the study. A model of iliofemoral stent implantation was used as previously described to study endothelialization and inflammatory reaction after stenting.[12] Animals received aspirin (40 mg) orally 12 hours before stent implantation and until euthanasia. Immediately after bilateral iliac artery endothelial balloon denudation, devices were deployed in the denuded section of the left and right iliac arteries. Animals were randomly allocated to 4 treatment groups (EES, bEES, BES, and BMS, n=6 per group at 14 and 28 days). Standard follow-up angiography using contrast media was performed to confirm stent patency
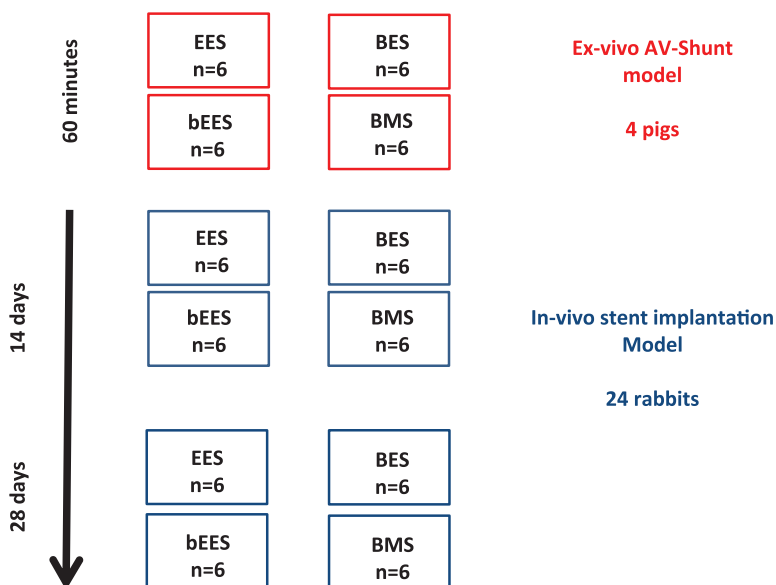


**Figure 1.** Study flow chart. EES (n=6 in the porcine model, n=12 in the rabbit model) denotes biodegradable polymer metallic everolimus-eluting stent. bEES (n=6 in the porcine model, n=12 in the rabbit model) denotes fully bioabsorbable everolimus-eluting stent. BES (n=6 in the porcine model, n=12 in the rabbit model) denotes biodegradable polymer metallic biolimus-eluting stent. BMS (n=6 in the porcine model, n=12 in the rabbit model) denotes bare metal stent.

before euthanasia at 14 and 28 days, respectively. After euthanasia, iliac arteries were perfusion-fixed at physiological pressure using 10% neutral buffered formalin, harvested, and bisected longitudinally. The specimens were prepared for confocal microscopy (CM) and scanning electron microscopy (SEM) analysis. The experimental set-up is detailed in methods in the the Data Supplement.

## Immunostaining and Imaging Procedures

In the shunt model, one stent half was immunostained using platelet markers (CD61, Immunotech, Commerce, CA; dilution 1:100, and CD42b, Santa Cruz, Dallas, TX; dilution 1:40) relevant for thrombocyte adhesion and aggregation and examined en face by CM and by SEM after completion of CM image acquisition, whereas the other half was processed for immunostaining using inflammatory markers (CD14, Novus Biological, Littleton, CO; dilution 1:40 and PM-1, BMA Biological, Littleton, CO; dilution 1:800) and examined en face by CM. The positive area of platelet staining was analyzed by proprietary software (Zeiss ZEN 2012, Carl-Zeiss Microscopy, Jena, Germany) within predefined regions of interest (40 mm$^2$), which was applied to all examined samples. Data are reported as area staining positive for CD61/42b (mm$^2$) within each region of interest and as percent fluorescent positive area within the entire stented segment. The imaging protocol is detailed in methods in the Data Supplement.

In the rabbit model, one half of the stented artery was processed for CD31/PECAM-1 (Dako, Carpenteria, CA, dilution 1:20) immunostaining and the opposite side reserved for RAM-11 (Dako, Carpenteria, CA, dilution 1:400) immunostaining. Both sides were imaged en face on a Zeiss LSM 700 laser confocal microscope (Carl-Zeiss Microscopy, Jena, Germany) at 5× magnification with tiled Z-stack technology for whole surface view and at 20× magnification with single Z-stack for local regions of interest. Semi-quantification of CD31/PECAM-1–positive endothelial cells was achieved by visual assessment above and between stent struts and expressed as median with lower (25th percentile) and upper quartiles (75th percentile). Details of the analysis are further explained in the methods in the Data Supplement. Subsequently, the CD31-stained half of the stented artery was processed for SEM after acquisition of CM images.

## Statistical Analysis

Variables were first checked for normal distribution using the Lilliefors corrected Kolmogorow–Smirnow test, then separated into variables with normal and non-normal distribution. Mean values with standard deviation were derived from normally distributed parameters, whereas non-normally distributed data were described as median with 25% and 75% percentiles. The Kruskal–Wallis test with Dunnett's post hoc correction was used for comparison of non-normally distributed data, whereas analysis of variance with Dunnett's post hoc correction was used for normally distributed data. A value of $P \leq 0.05$ was considered statistically significant. For the porcine ex vivo arterio-venous shunt model, nested generalized linear mixed models with Dunnett's correction for multiple testing were used to investigate group differences in consideration of multiple measurements per individual. Within these models, stent type was considered as fixed effect, whereas the experimental factor variables animal and shunt position were considered as nested random effects. Covariance type was set to autoregressive order 1. The analyses were performed with SPSS Advanced Statistics Version 22 (IBM, Armonk, New York). The statistical tests were 2-tailed and a value of $P < 0.05$ was considered to indicate statistical significance.

## Results

### Acute Thrombogenicity in a Porcine AV Shunt Model

All animals survived the study's in-life-phase. Shunts ran an average of 58.8±3.5 minutes.

Platelet aggregation as detected by CM (CD61 and CD42b) demonstrated a significantly lower mean percentage of fluorescent positive area in the EES as compared with bEES, BES, and BMS. Representative images of relative and absolute platelet coverage area based on fluorescent staining against CD61 and CD42b are shown in Figure 2. Linear mixed-effects model procedures demonstrated biologically
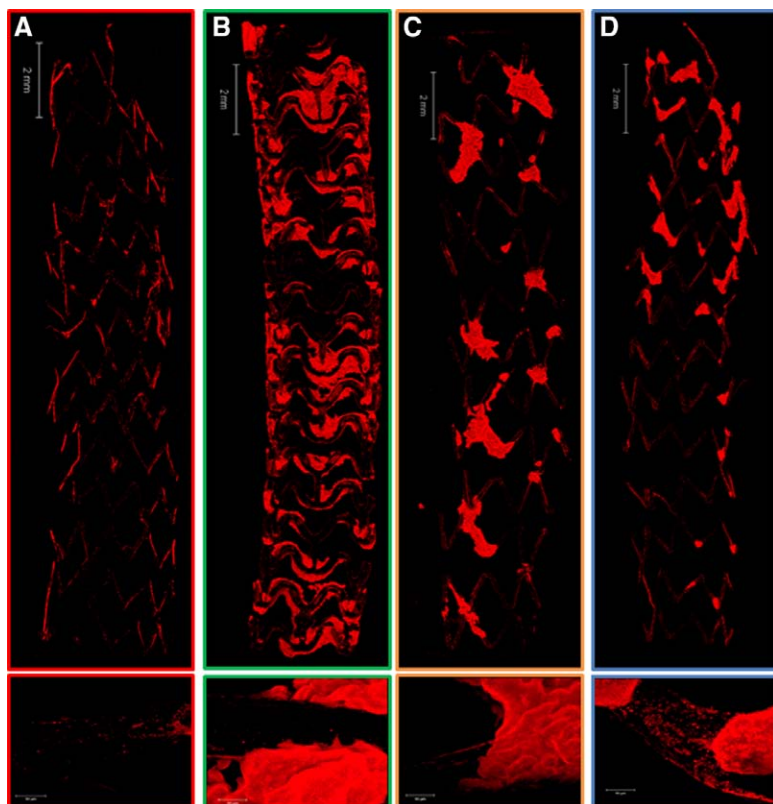


**Figure 2.** Ex-vivo arteriovenous porcine shunt model. Representative images derived from confocal microscopy after 1 hour in a swine ex vivo shunt model at low (10×) and high (20×) magnification. **A**, Shows biodegradable polymer metallic everolimus eluting stent (EES) (n=6). **B**, Shows fully bioabsorbable everolimus eluting stent (bEES) (n=6). **C**, Shows biodegradable polymer metallic biolimus eluting stent (n=6). **D**, Shows bare metal stent (BMS) (n=6).
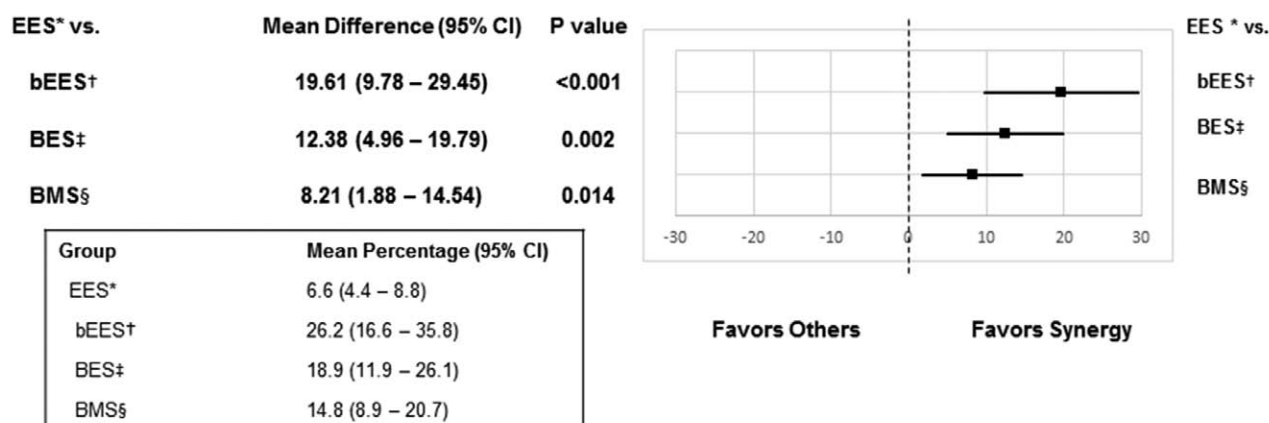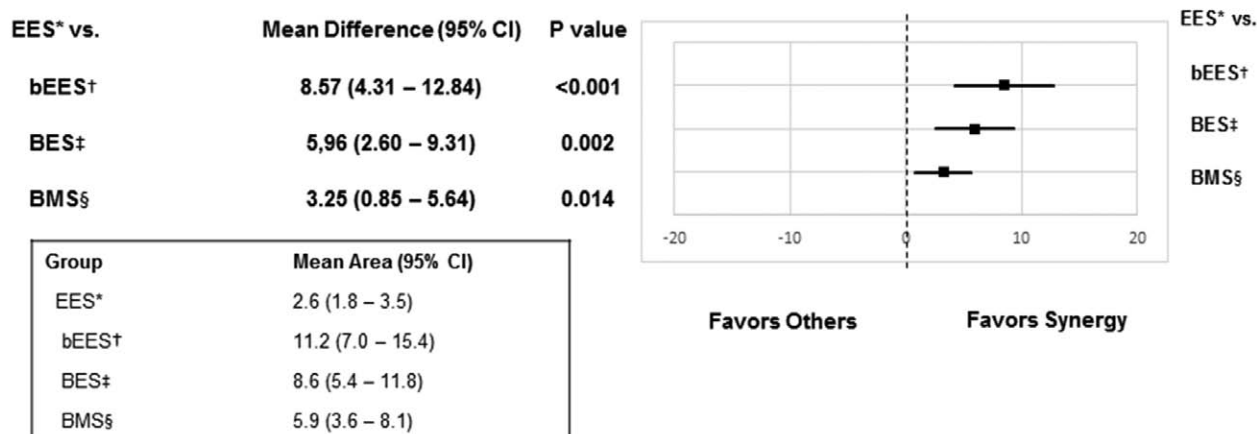
## A  Percent fluorescent positive area (% adherent platelets)

| EES* vs. | Mean Difference (95% CI) | P value |
|---|---|---|
| bEES† | 19.61 (9.78 – 29.45) | <0.001 |
| BES‡ | 12.38 (4.96 – 19.79) | 0.002 |
| BMS§ | 8.21 (1.88 – 14.54) | 0.014 |

| Group | Mean Percentage (95% CI) |
|---|---|
| EES* | 6.6 (4.4 – 8.8) |
| bEES† | 26.2 (16.6 – 35.8) |
| BES‡ | 18.9 (11.9 – 26.1) |
| BMS§ | 14.8 (8.9 – 20.7) |

Favors Others          Favors Synergy

## B  Fluorescent positive area (adherent platelets in mm²)

| EES* vs. | Mean Difference (95% CI) | P value |
|---|---|---|
| bEES† | 8.57 (4.31 – 12.84) | <0.001 |
| BES‡ | 5,96 (2.60 – 9.31) | 0.002 |
| BMS§ | 3.25 (0.85 – 5.64) | 0.014 |

| Group | Mean Area (95% CI) |
|---|---|
| EES* | 2.6 (1.8 – 3.5) |
| bEES† | 11.2 (7.0 – 15.4) |
| BES‡ | 8.6 (5.4 – 11.8) |
| BMS§ | 5.9 (3.6 – 8.1) |

Favors Others          Favors Synergy

**Figure 3.** Ex-vivo arteriovenous shunt model. **A**, Percent fluorescent positive area based on percentage of fluorescent positive staining against CD61 and CD42b within the entire stented segment. Values are expressed as mean group differences relative to EES with 95% confidence interval and as mean percentage with 95% confidence interval. EES*, bEES†, and BMS§ constitute of n=6 stents in each group, whereas BES‡ constitute of n=5 stents. One BES was incompletely expanded and therefore not included in the analysis. **B**, Absolute fluorescent positive area based on area of fluorescent positive staining against CD61 and CD42b within the bisected stented segment expressed as group differences relative to EES. Values are mean difference with 95% confidence interval and as mean area with 95% confidence interval. CI indicates confidence interval. EES*, bEES†, and BMS§ constitute of n=6 stents in each group, whereas BES‡ constitute of n=5 stents. One BES was incompletely expanded and therefore not included in the analysis. bEES indicates fully bioabsorbable everolimus-eluting stent; BES, biodegradable polymer metallic biolimus-eluting stent; BMS denotes bare metal stent; and EES, biodegradable polymer metallic everolimus-eluting stent.

relevant and statistically significant differences in percent and absolute positive fluorescence area between EES versus bEES ($P<0.001$), BES ($P=0.002$), and BMS ($P=0.014$) as shown in Figure 3. Percent acute inflammatory cell adhesion in stents based on fluorescent staining against monocyte marker CD14 and neutrophil marker PM1 are shown in Figure IA and IB in the Data Supplement as median with lower (25th percentile) and upper quartiles (75th percentile). With respect to CD14-positive inflammatory cell adhesion, EES demonstrated significantly less positive cell counts than bEES ($P=0.043$). Also, EES had fewer PM1-positive neutrophils adherent compared with the other devices (Table I in the Data Supplement).

### Re-Endothelialization After Arterial Denudation in Healthy Rabbit Iliac Arteries

All rabbits survived the study's in-life-phase. All stents were found evenly expanded against the arterial wall and patent

without evidence of stent fracture. Quantification of endothelial coverage above struts by SEM was numerically greater in EES compared with bEES at 14 days ($P=0.15$) and lower when compared with control BMS ($P=0.27$) as shown in the Table. The percentage of endothelial coverage by CM evaluating CD31/PECAM-1 staining was also numerically higher in EES when compared with bEES ($P=0.55$) and lower when compared with BMS ($P=0.15$) at 14 days. No differences were observed between EES and BES. Quantitative results of endothelial coverage by CM above and between struts are detailed in Figure 4 and Table II in the Data Supplement.

At 28 days, SEM revealed significantly greater endothelial coverage above struts in EES as compared with bEES ($P=0.05$). No differences were observed between EES and BES. For control BMS, endothelial coverage was near complete above struts (Table). CM of CD31/PECAM-1 staining showed endothelial coverage above struts was numerically

greater in EES as compared with bEES (*P*=0.20). However, no significant differences were observed between bEES, BES, BMS, and EES (Table II in the Data Supplement). Representative images of endothelial coverage at 14 and 28 days are shown in Figure 4.

Adhesion of RAM-11 positive macrophages was predominantly visualized in the surrounding of stent struts, where coverage with CD31/PECAM-1–positive endothelial cells was absent. Overall, RAM-11–positive macrophage adhesion was numerically lower in EES at 14 days compared with bEES (*P*=0.11) without significant differences observed between groups as shown in Table I in the Data Supplement and Figure IC and ID in the Data Supplement.

## Discussion

The current study examined acute thrombogenicity, reendothelialization and inflammatory reaction of thin-strut EES as compared with thick-strut bEES, thick-strut BES, and BMS. The aim was to characterize clinically meaningful end points relevant to vascular healing after implantation of contemporary coronary stents of different design and composition in well-established animal models. The most salient findings of our study are as follows:

1. Thin strut EES revealed significantly less platelet aggregation and inflammatory cell adhesion in a porcine AV shunt model as compared with bEES, BES, and BMS.
2. Re-endothelialization after arterial denudation and stent implantation was significantly greater in thin-strut EES as compared with bEES in a healthy rabbit iliac artery model at 28 days and was similar to BES. Only BMS showed near complete re-endothelialization at 28 days by SEM. CM analysis confirmed the differential pace of re-endothelialization, with incomplete endothelial maturation in all DES devices detected by CD31/PECAM-1–positive endothelial cells at 28 days. Adhesion of RAM-11–positive macrophages was significantly lower in thin-strut EES as compared with bEES at 14 days and was similar in BES. When compared with BMS, the presence of any (abluminal) polymer in combination with antiproliferative drug was associated with increased inflammation and decreased endothelialization in the rabbit model. The examination of isolated polymer coating effects on inflammatory cell adhesion and re-endothelialization was not intended in the current study set-up and warrants further investigation.

### Relevance of Stent Geometry and Polymer Coating for Acute Thrombogenicity

The importance of DES coating and strut dimensions relative to the vessel wall were recently described as critical factors affecting acute thrombogenicity in an in vitro flow-loop model.[6] Kolandaivelu et al showed that DES coated with permanent polymers uniformly decreased thrombus formation as compared with their BMS counterparts. However, the study investigated acute thrombogenicity in an in vitro closed flow loop model using blood collected from naïve 4-month-old Yorkshire pigs (36–40 kg). In their study, Kolandaivelu et al assessed clot adherence visually and measured lactate dehydrogenase to provide a semiquantitative measure of platelet aggregation. In this regard, our study may be more in line with what is expected acutely after stent deployment in human arteries because platelet reactivity in a flow-loop model may not appropriately replicate in vivo conditions. Although active release of immuno-modulatory drugs has

been shown to influence activation of distinct coagulation pathways in cell culture studies, it is unclear whether this phenomenon occurs in vivo.[13,14] A clinically relevant set-up was chosen for the current investigation, in which contemporary commercially available thick and thin-strut metallic DES with abluminal coating of biodegradable polymer and thick-strut fully bioabsorbable PLLA-based scaffolds, circumferentially coated with a different bioabsorbable PDLLA polymer coating releasing everolimus, were exposed to circulating blood in the absence of antiplatelet drugs to study thrombocyte adherence and aggregation under real-time in vivo conditions. In contrast to the above referenced study by Kolandaivelu et al, which exclusively used DES with a circumferential durable polymer coating adopted from first and second generation FDA-approved DES, our study used DES with an abluminal biodegradable polymer coating of differential strut thickness and geometry. Also, a comparative assessment of acute thrombogenicity in current generation DES and fully bioabsorbable vascular stents releasing everolimus from a biodegradable polymer matrix has not been performed to date.

It has been demonstrated in our study that thin-strut EES exhibit significantly less platelet aggregation and accelerated endothelial recovery as compared with bEES and thick-strut BES. In a previous study, Eppihimer et al determined acute thrombus formation in a closed loop system, in which stents made of PtCr were exposed to human blood under physiological shear rates in the presence or absence of polyvinylidene fluoride-co-hexafluoropropene (PVDF-HFP) polymer coating.[15] In that study, PtCr stents exhibited significantly less thrombus formation when compared with their PVDF-HFP coated counterparts,[15] which may partly explain the favorable outcomes of the thin-strut EES made from a PtCr alloy in the current study. Although studies by Kolandaivelu and Eppihimer used customized stent designs to specifically address the comparative influence of stent components on vascular healing, we sought to characterize the integrated performance of clinically used devices rather than to decipher the effect of individual stent components.

The results of the current study further emphasize the importance of stent geometry and flow dynamics with regard to activation of coagulatory pathways and re-endothelialization. Thick-strut fully bioabsorbable bEES showed increased acute thrombogenicity. This phenomenon can be explained by augmented flow alterations arising from bulky stent struts when compared with thin-strut DES like the EES tested in our study. Landmark findings of prior clinical studies addressing the impact of stent design support this finding,[16] which becomes even more significant in the setting of incomplete apposition to the vessel wall, what seemed to be an important risk factor for ST in human autopsy cases.[17] Therefore, there is no doubt that features of stent geometry affect coronary blood flow dynamics and should be carefully considered in the design of novel metallic and bioabsorbable stents.

### Relevance of Acute Inflammation for Thrombus Formation

Arterial thrombosis in atherosclerotic lesions is prone to occur in the presence of activated plaque-derived tissue-factor[18] and has historically been proposed to be the predominant activator

**Table.    Rabbit Model**

| Endothelial Coverage by SEM | | | | Median | Percentile 25th | Percentile 75th | P Value |
|---|---|---|---|---|---|---|---|
| 14 days | Above struts, % | Biodegradable polymer metallic everolimus-eluting stent (EES) | n=6 | 19.8 | 16.5 | 44.0 | |
| | | Fully bioabsorbable everolimus-eluting stent (bEES) | n=6 | 0.7 | 0.5 | 1.8 | EES vs bEES; P=0.15 |
| | | Biodegradable polymer metallic biolimus-eluting stents (BES) | n=6 | 17.9 | 2.9 | 33.8 | EES vs BES; P=1.00 |
| | | Bare metal stents (BMS) | n=6 | 91.1 | 82.1 | 96.8 | EES vs BMS; P=0.27 |
| | Between struts, % | Biodegradable polymer metallic everolimus-eluting stent (EES) | n=6 | 90.4 | 88.0 | 92.1 | |
| | | Fully bioabsorbable everolimus-eluting stent (bEES) | n=6 | 89.1 | 82.1 | 89.7 | EES vs bEES; P=0.29* |
| | | Biodegradable polymer metallic biolimus-eluting stents (BES) | n=6 | 88.7 | 87.1 | 89.8 | EES vs BES; P=0. 75* |
| | | Bare metal stents (BMS) | n=6 | 96.8 | 93.8 | 98.7 | EES vs BMS; P=0.005* |
| 28 days | Above struts, % | Biodegradable polymer metallic everolimus-eluting stent (EES) | n=6 | 87.5 | 74.0 | 93.3 | |
| | | Fully bioabsorbable everolimus-eluting stent (bEES) | n=6 | 12.4 | 8.3 | 19.3 | EES vs bEES; P=0.05 |
| | | Biodegradable polymer metallic biolimus-eluting stents (BES) | n=6 | 67.5 | 51.9 | 82.1 | EES vs BES; P=1.00 |
| | | Bare metal stents (BMS) | n=6 | 100 | 99.7 | 100 | EES vs BMS; P=0.51 |
| | Between struts, % | Biodegradable polymer metallic everolimus-eluting stent (EES) | n=6 | 97.7 | 96.9 | 98.0 | |
| | | Fully bioabsorbable everolimus-eluting stent (bEES) | n=6 | 95.1 | 93.3 | 95.3 | EES vs bEES; P=0.45 |
| | | Biodegradable polymer metallic biolimus-eluting stents (BES) | n=6 | 95 | 94.1 | 95.4 | EES vs BES; P=0.38 |
| | | Bare metal stents (BMS) | n=6 | 100 | 100 | 100 | EES vs BMS; P=0.54 |

Percentage endothelial coverage by visual estimation derived from SEM images after 14 and 28 days. Values represent median with lower (25th percentile) and upper quartiles (75th percentile). EES (n=6 at 14 days, n=6 at 28 days) denotes biodegradable polymer metallic everolimus-eluting stent. bEES (n=6 at 14 days, n=6 at 28 days) denotes fully bioabsorbable everolimus-eluting stent. BES (n=6 at 14 days, n=6 at 28 days) denotes biodegradable polymer metallic biolimus-eluting stent. BMS (n=6 at 14 days, n=6 at 28 days) denotes bare metal stent. ANOVA indicates analysis of variance; and SEM, scanning electron microscopy.

*ANOVA with Dunnett post hoc correction.

of the coagulation cascade.[19] To date, the precise role of circulating acute inflammatory cells that may lead to thrombus formation in the absence of substantial tissue injury is unclear. An inherent role of tissue factor derived from blood-born inflammatory cells in the context of arterial thrombosis and its specific contribution to enhanced coagulation has been shown in an experimental study on human leukocytes.[20] This study demonstrated that atherosclerotic lesions may be inclined toward arterial thrombosis from the accumulation of circulating inflammatory cells. Human blood–derived neutrophils and monocytes have been shown to be an important source of tissue-factor to initiate coagulation pathways.[20] On a more molecular level, leukocytes are further capable of transferring tissue-factor to platelets using CD15 receptors, forming procoagulatory platelet aggregates containing leukocyte-derived tissue factor.[21]

In our study, we found increased adherence of acute inflammatory cells in thick-strut bEES as compared with thin-strut EES. Despite the substantial difference in strut thickness among the currently tested devices and its relevance in inflammatory cell adhesion,[10] polymer coating specifics may play an equipollent role in this regard and should be considered during development of these devices.

## Impact of Stent Design on Endothelial Regrowth and Maturity

Delayed endothelial recovery has been identified as one of the major contributing factors of late stent thrombosis at autopsy.[1,2] In a previous study, we showed disparities in the rate of endothelialization of first and second generation durable polymer-based DES, supporting enhanced vascular healing properties in thin-strut second generation DES, when compared with thick-strut first generation devices.[22] Similarly, re-endothelialization was delayed in thick-strut bEES as compared with thin-strut EES in the current study owing to an incremental delay in cellular repopulation of bulky stent struts in the former. Stent designs are known to influence endothelial growth by altering shear stress and blood flow dynamics.[23,24] In an experimental setting with flow and shear conditions similarly monitored in arteries, endothelial coverage was found to depend on object thickness.[25] Simon et al showed that endothelial cell coverage area and migration distance significantly decreased in objects with 75 μm thickness or greater, which would explain the delayed endothelial coverage thick-strut bEES (150 μm) observed in our study.[25]
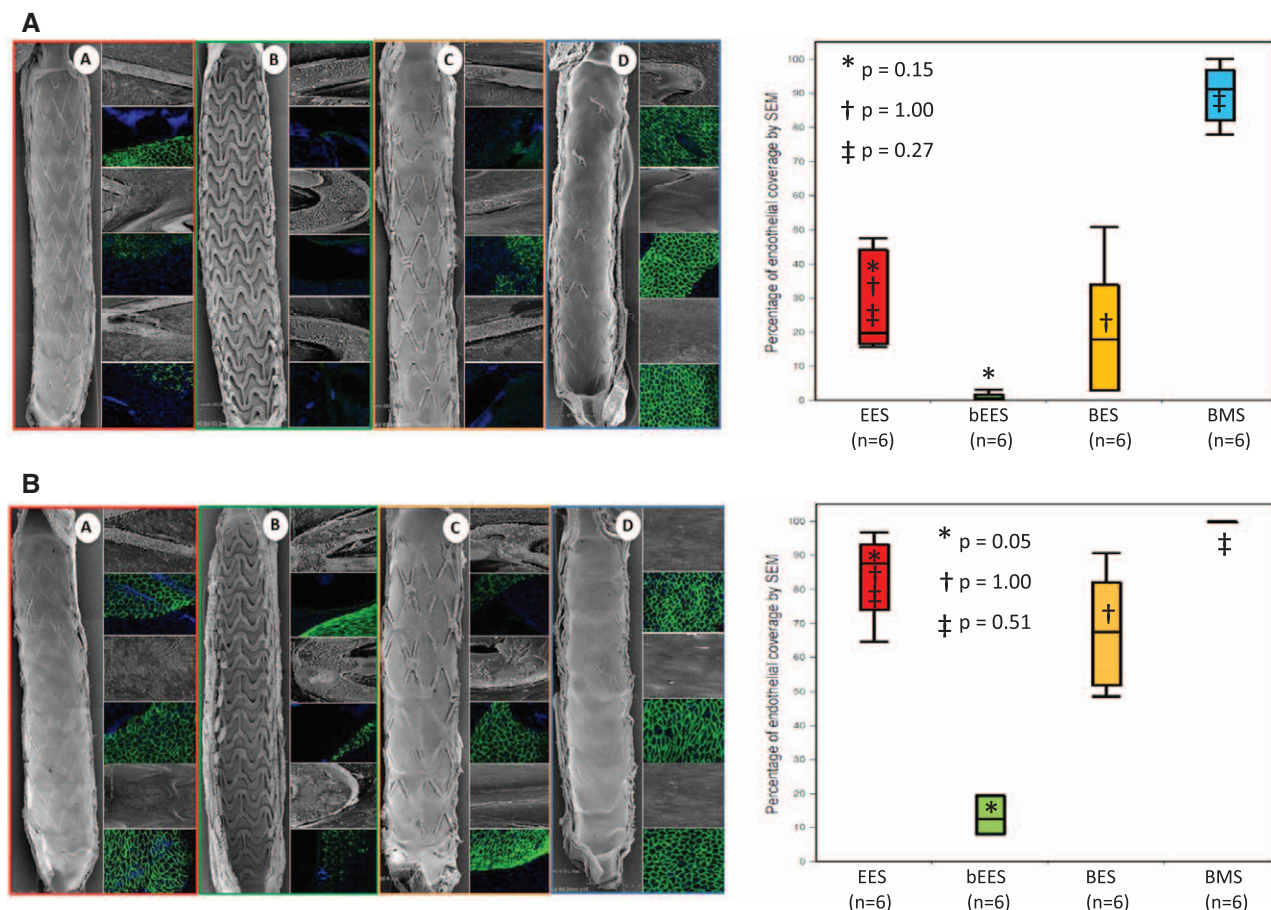
**Figure 4.** Rabbit model. Representative images of endothelial coverage assessed by scanning electron microscopy at 14 days (**A**) and 28 days (**B**). Low magnification (15×) Scanning electron microscopy (SEM) images provide an overview of the luminal surface of the bisected segment from proximal (**top**) to distal (**bottom**). High magnification (200×) SEM images and confocal microscopy images based on CD31/PECAM-1 expression are depicted from proximal (**top**), mid (**middle**), and distal (**bottom**) stented regions. **A**, Shows biodegradable polymer metallic everolimus eluting stent (EES) (n=6). **B**, Shows fully bioabsorbable everolimus eluting stent (bEES) (n=6). **C**, Shows biodegradable polymer metallic biolimus eluting stent (n=6). **D**, Shows bare metal stent (BMS) (n=6). Relative percentage of endothelial coverage above struts assessed by scanning electron microscopy is shown in box and whisker diagrams on the right. Values represent median with lower (25th percentile) and upper quartiles (75th percentile) and whiskers for minimum and maximum value. EES (n=6) denotes biodegradable polymer metallic everolimus-eluting stent. bEES (n=6) denotes fully bioabsorbable everolimus-eluting stent. BES (n=6) denotes biodegradable polymer metallic biolimus-eluting stent. BMS (n=6) denotes bare metal stent.

Although strut dimensions have been shown to affect endothelialization rates, inherent surface properties must also be considered when evaluating endothelialization rates among contemporary coronary stents. Durable PVDF-HFP polymer surfaces are associated with lower endothelial cell coverage and maturity in the early phase after stent placement when compared with bare PtCr metallic stent surfaces used in the thin-strut biodegradable polymer EES.[15] However, these findings were observed in the absence of drug and may not be applicable to commercially available DES. In another experimental study, endothelialization of 2 durable polymers, poly(ethylene-co-vinylacetate) and poly(butyl methacrylate) was reduced, whereas enhanced endothelial coverage was observed in biodegradable polymers, namely PLLA, poly(3-hydroxybutyrate), poly(4-hydroxybutyrate), and a polymeric blend of PLLA/poly(4-hydroxybutyrate), tested in in vitro cultures using human umbilical endothelial cells.[26] These observations reinforce a potential role of polymeric coating influencing the kinetics of endothelial cell recovery.

Although polymer coatings and stent geometry undisputedly impact endothelial recovery after stent implantation, the most pertinent factor is likely the release of potent antiproliferative drugs. Considering the complex nature of contemporary DES, pharmacokinetic profile and drug dose are also likely driving factors of endothelial recovery after implantation in diseased coronary arteries. Despite the importance of stent design in modulating re-endothelialization, the drug exerts a profound pharmacological effect and clearly also plays a crucial role.

### Implications for Clinical Practice

Stent thrombosis (ST) remains a clinically relevant issue complicated by increased mortality and morbidity, despite the introduction of newer generation DES.[27] Advanced dual antiplatelet therapy, stent design, and emphasis on optimal stent implantation techniques have helped reduce clinical event rates to ≈1.0% to 1.5% in contemporary practice.[27,28] Nonetheless, ST rates are still high in certain clinical settings with increased procoagulatory activity, such as acute myocardial

infarction, even with the use of newer generation devices and modern antiplatelet therapy. In a similar vein, an autopsy study from our registry highlighted the impact of thrombus burden and suboptimal stent implantation in unstable lesions triggering early ST, suggesting that refining implantation techniques and stent design might improve clinical outcomes of ACS patients.[17]

Although procoagulatory condition and suboptimal implantation are the main factors in the development of ST during the first 30 days after implantation,[17] delayed endothelial recovery and peri-strut inflammatory response are known stimuli for the risk of late and very late stent thrombosis.[2] The LEADERS (Limus Eluted From a Durable Versus Erodable Stent Coating) trial showed a rate of definitive/probable late and very late ST in biodegradable polymer BES of 0.6% and 0.9%, respectively, after 5 years, which was significantly less as compared with thick-strut first generation sirolimus-eluting stents with a very late ST rate of 2.9% at 5 years.[29] Randomized clinical trial results evaluating very late stent thrombosis in the newer generation thin-strut EES that may even further reduce event rates have not been published to date.

With the advent of fully bioabsorbable devices, fully bioresorbable bEES are increasingly used in a variety of different clinical settings including acute coronary syndrome.[30–32] Yet, robust data from randomized clinical trials are lacking for these devices. Early ST rates of 1.5% and cumulative ST rates of 2.1% at 6 months of follow-up are reported from the European GHOST registry in the bEES.[33] The clinical manifestation of early ST is based on a complex interaction of device-, procedure-, and patient-related factors. However, extensive preclinical and clinical testing of the prothrombotic effects of bioabsorbable vascular implants is warranted to improve this technology. Transferability of the utilized animal models to human disease conditions is crucial to facilitate understanding of device-related effects on clinically relevant end points, such as acute thrombogenicity and re-endothelialization. Although the combination of previously established animal models investigating different biological sequences of vascular healing was thought to deliver insightful differences among the investigated devices, clinical studies are needed to delineate their relative merits.

## Limitations

The examination of DES implants in rabbits was done at 14 and 28 days. It is unclear whether longer-term follow up may reveal differential healing characteristics of these contemporary devices. Moreover, it is important to understand that experimental studies, such as the current one, can only address limited aspects contributing to thrombogenicity and endothelialization but cannot reproduce the complexity of human disease conditions. We studied acute thrombogenicity and re-endothelialization among contemporary DES and bioresorbable stents in a healthy rabbit model. Therefore, the current findings have to be interpreted with caution when it comes to extrapolation to atherosclerotic disease conditions. Although strut thickness and differences in stent design likely play an important role in the determination of acute thrombogenicity and vascular healing, the current study was not designed to decipher individual stent components and their relevance for the chosen end points.

## Conclusions

In comparison to selected contemporary thick-strut metallic biodegradable polymer and fully bioabsorbable DES, the thin-strut biodegradable polymer metallic EES demonstrated decreased acute thrombogenicity with respect to platelet aggregation and inflammatory cell adhesion while fostering enhanced endothelial recovery.

## Disclosures

Dr Feygin is an employee of Boston Scientific Corporation, Marlborough, MA. Dr Joner is a consultant for Biotronik and Cardionovum and has received speaking honorarium from Abbott Vascular, Biotronik, Medtronic, and St Jude. Dr Virmani receives research support from Abbott Vascular, BioSensors International, Biotronik, Boston Scientific, Medtronic, MicroPort Medical, OrbusNeich Medical, SINO Medical Technology, and Terumo Corporation; has speaking engagements with Merck; receives honoraria from Abbott Vascular, Boston Scientific, Lutonix, Medtronic, and Terumo Corporation; and is a consultant for 480 Biomedical, Abbott Vascular, Medtronic, and W.L. Gore. The other authors report no conflicts.

## References

1. Joner M, Finn AV, Farb A, Mont EK, Kolodgie FD, Ladich E, Kutys R, Skorija K, Gold HK, Virmani R. Pathology of drug-eluting stents in humans: delayed healing and late thrombotic risk. *J Am Coll Cardiol*. 2006;48:193–202. doi: 10.1016/j.jacc.2006.03.042.
2. Finn AV, Joner M, Nakazawa G, Kolodgie F, Newell J, John MC, Gold HK, Virmani R. Pathological correlates of late drug-eluting stent thrombosis: strut coverage as a marker of endothelialization. *Circulation*. 2007;115:2435–2441. doi: 10.1161/CIRCULATIONAHA.107.693739.
3. Byrne RA, Joner M, Tada T, Kastrati A. Restenosis in bare metal and drug-eluting stents: distinct mechanistic insights from histopathology and optical intravascular imaging. *Minerva Cardioangiol*. 2012;60:473–489.
4. Palmerini T, Biondi-Zoccai G, Della Riva D, Stettler C, Sangiorgi D, D'Ascenzo F, Kimura T, Briguori C, Sabatè M, Kim HS, De Waha A, Kedhi E, Smits PC, Kaiser C, Sardella G, Marullo A, Kirtane AJ, Leon MB, Stone GW. Stent thrombosis with drug-eluting and bare-metal stents: evidence from a comprehensive network meta-analysis. *Lancet*. 2012;379:1393–1402. doi: 10.1016/S0140-6736(12)60324-9.
5. Sabate M, Cequier A, Iñiguez A, Serra A, Hernandez-Antolin R, Mainar V, Valgimigli M, Tespili M, den Heijer P, Bethencourt A, Vazquez N, Gómez-Hospital JA, Baz JA, Martin-Yuste V, van Geuns RJ, Alfonso F, Bordes P, Tebaldi M, Masotti M, Silvestro A, Backx B, Brugaletta S, van Es GA, Serruys PW. Everolimus-eluting stent versus bare-metal stent in ST-segment elevation myocardial infarction (EXAMINATION): 1 year results of a randomised controlled trial. *Lancet*. 2012;380:1482–1490. doi: 10.1016/S0140-6736(12)61223-9.
6. Kolandaivelu K, Swaminathan R, Gibson WJ, Kolachalama VB, Nguyen-Ehrenreich KL, Giddings VL, Coleman L, Wong GK, Edelman ER. Stent thrombogenicity early in high-risk interventional settings is driven by stent design and deployment and protected by polymer-drug coatings. *Circulation*. 2011;123:1400–1409. doi: 10.1161/CIRCULATIONAHA.110.003210.
7. Stefanini GG, Kalesan B, Serruys PW, Heg D, Buszman P, Linke A, Ischinger T, Klauss V, Eberli F, Wijns W, Morice MC, Di Mario C, Corti R, Antoni D, Sohn HY, Eerdmans P, van Es GA, Meier B, Windecker S, Jüni P. Long-term clinical outcomes of biodegradable polymer biolimus-eluting stents versus durable polymer sirolimus-eluting stents in patients with coronary artery disease (LEADERS): 4 year follow-up of a randomised non-inferiority trial. *Lancet*. 2011;378:1940–1948. doi: 10.1016/S0140-6736(11)61672-3.
8. Stefanini GG, Byrne RA, Serruys PW, de Waha A, Meier B, Massberg S, Jüni P, Schömig A, Windecker S, Kastrati A. Biodegradable polymer drug-eluting stents reduce the risk of stent thrombosis at 4 years in patients undergoing

percutaneous coronary intervention: a pooled analysis of individual patient data from the ISAR-TEST 3, ISAR-TEST 4, and LEADERS randomized trials. *Eur Heart J*. 2012;33:1214–1222. doi: 10.1093/eurheartj/ehs086.

9. Serruys PW, Chevalier B, Dudek D, Cequier A, Carrié D, Iniguez A, Dominici M, van der Schaaf RJ, Haude M, Wasungu L, Veldhof S, Peng L, Staehr P, Grundeken MJ, Ishibashi Y, Garcia-Garcia HM, Onuma Y. A bioresorbable everolimus-eluting scaffold versus a metallic everolimus-eluting stent for ischaemic heart disease caused by de-novo native coronary artery lesions (ABSORB II): an interim 1-year analysis of clinical and procedural secondary outcomes from a randomised controlled trial. *Lancet*. 2015;385:43–54. doi: 10.1016/S0140-6736(14)61455-0.

10. Chin-Quee SL, Hsu SH, Nguyen-Ehrenreich KL, Tai JT, Abraham GM, Pacetti SD, Chan YF, Nakazawa G, Kolodgie FD, Virmani R, Ding NN, Coleman LA. Endothelial cell recovery, acute thrombogenicity, and monocyte adhesion and activation on fluorinated copolymer and phosphorylcholine polymer stent coatings. *Biomaterials*. 2010;31:648–657. doi: 10.1016/j.biomaterials.2009.09.079.

11. National Research Council Committee for the Update of the Guide for the Care and Use of Laboratory Animals. *Guide for the Care and Use of Laboratory Animals*. 8th ed. Washington, DC: The National Academies Press; 2011.

12. Yazdani SK, Sheehy A, Nakano M, Nakazawa G, Vorpahl M, Otsuka F, Donn RS, Perkins LE, Simonton CA, Kolodgie FD, Virmani R. Preclinical evaluation of second-generation everolimus- and zotarolimus-eluting coronary stents. *J Invasive Cardiol*. 2013;25:383–390.

13. Weyrich AS, Denis MM, Schwertz H, Tolley ND, Foulks J, Spencer E, Kraiss LW, Albertine KH, McIntyre TM, Zimmerman GA. mTOR-dependent synthesis of Bcl-3 controls the retraction of fibrin clots by activated human platelets. *Blood*. 2007;109:1975–1983. doi: 10.1182/blood-2006-08-042192.

14. Aslan JE, Tormoen GW, Loren CP, Pang J, McCarty OJ. S6K1 and mTOR regulate Rac1-driven platelet activation and aggregation. *Blood*. 2011;118:3129–3136. doi: 10.1182/blood-2011-02-331579.

15. Eppihimer MJ, Sushkova N, Grimsby JL, Efimova N, Kai W, Larson S, Forsyth B, Huibregtse BA, Dawkins KD, Wilson GJ, Granada JF. Impact of stent surface on thrombogenicity and vascular healing: a comparative analysis of metallic and polymeric surfaces. *Circ Cardiovasc Interv*. 2013;6:370–377. doi: 10.1161/CIRCINTERVENTIONS.113.000120.

16. Rogers C, Edelman ER. Endovascular stent design dictates experimental restenosis and thrombosis. *Circulation*. 1995;91:2995–3001.

17. Nakano M, Yahagi K, Otsuka F, Sakakura K, Finn AV, Kutys R, Ladich E, Fowler DR, Joner M, Virmani R. Causes of early stent thrombosis in patients presenting with acute coronary syndrome: an ex vivo human autopsy study. *J Am Coll Cardiol*. 2014;63:2510–2520. doi: 10.1016/j.jacc.2014.02.607.

18. Palmerini T, Tomasi L, Barozzi C, Della Riva D, Mariani A, Taglieri N, Leone O, Ceccarelli C, De Servi S, Branzi A, Genereux P, Stone GW, Ahamed J. Detection of tissue factor antigen and coagulation activity in coronary artery thrombi isolated from patients with ST-segment elevation acute myocardial infarction. *PLoS One*. 2013;8:e81501. doi: 10.1371/journal.pone.0081501.

19. Fuster V, Fallon JT, Nemerson Y. Coronary thrombosis. *Lancet*. 1996;348(suppl 1):s7–s10.

20. Giesen PL, Rauch U, Bohrmann B, Kling D, Roqué M, Fallon JT, Badimon JJ, Himber J, Riederer MA, Nemerson Y. Blood-borne tissue factor: another view of thrombosis. *Proc Natl Acad Sci U S A*. 1999;96:2311–2315.

21. Rauch U, Bonderman D, Bohrmann B, Badimon JJ, Himber J, Riederer MA, Nemerson Y. Transfer of tissue factor from leukocytes to platelets is mediated by CD15 and tissue factor. *Blood*. 2000;96:170–175.

22. Joner M, Nakazawa G, Finn AV, Quee SC, Coleman L, Acampado E, Wilson PS, Skorija K, Cheng Q, Xu X, Gold HK, Kolodgie FD, Virmani R. Endothelial cell recovery between comparator polymer-based drug-eluting stents. *J Am Coll Cardiol*. 2008;52:333–342. doi: 10.1016/j.jacc.2008.04.030.

23. LaDisa JF Jr, Olson LE, Douglas HA, Warltier DC, Kersten JR, Pagel PS. Alterations in regional vascular geometry produced by theoretical stent implantation influence distributions of wall shear stress: analysis of a curved coronary artery using 3D computational fluid dynamics modeling. *Biomed Eng Online*. 2006;5:40. doi: 10.1186/1475-925X-5-40.

24. Richter Y, Edelman ER. Cardiology is flow. *Circulation*. 2006;113:2679–2682. doi: 10.1161/CIRCULATIONAHA.106.632687.

25. Simon C, Palmaz JC, Sprague EA. Influence of topography on endothelialization of stents: clues for new designs. *J Long Term Eff Med Implants*. 2000;10:143–151.

26. Busch R, Strohbach A, Rethfeldt S, Walz S, Busch M, Petersen S, Felix S, Sternberg K. New stent surface materials: the impact of polymer-dependent interactions of human endothelial cells, smooth muscle cells, and platelets. *Acta Biomater*. 2014;10:688–700. doi: 10.1016/j.actbio.2013.10.015.

27. Mauri L, Hsieh WH, Massaro JM, Ho KK, D'Agostino R, Cutlip DE. Stent thrombosis in randomized clinical trials of drug-eluting stents. *N Engl J Med*. 2007;356:1020–1029. doi: 10.1056/NEJMoa067731.

28. Kufner S, Byrne RA, Valeskini M, Schulz S, Ibrahim T, Hoppmann P, Schneider S, Laugwitz KL, Schunkert H, Kastrati A. Five-year outcomes from a trial of three limus-eluting stents with different polymer coatings in patients with coronary artery disease: final results from the ISAR-TEST 4 randomised trial [published online ahead of print November 12, 2014]. *EuroIntervention*. doi: 10.4244/EIJY14M11_02.

29. Serruys PW, Farooq V, Kalesan B, de Vries T, Buszman P, Linke A, Ischinger T, Klauss V, Eberli F, Wijns W, Morice MC, Di Mario C, Corti R, Antoni D, Sohn HY, Eerdmans P, Rademaker-Havinga T, van Es GA, Meier B, Jüni P, Windecker S. Improved safety and reduction in stent thrombosis associated with biodegradable polymer-based biolimus-eluting stents versus durable polymer-based sirolimus-eluting stents in patients with coronary artery disease: final 5-year report of the LEADERS (Limus Eluted From A Durable Versus ERodable Stent Coating) randomized, noninferiority trial. *JACC Cardiovasc Interv*. 2013;6:777–789. doi: 10.1016/j.jcin.2013.04.011.

30. Ielasi A, Cortese B, Varricchio A, Tespili M, Sesana M, Pisano F, Loi B, Granata F, Moscarella E, Silva Orrego P, La Vecchia L, Steffenino G. Immediate and midterm outcomes following primary PCI with bioresorbable vascular scaffold implantation in patients with ST-segment myocardial infarction: insights from the multicentre "Registro ABSORB Italiano" (RAI registry) [published online ahead of print October 30, 2014]. *EuroIntervention*. doi 10.4244/EIJY14M10_11.

31. Gori T, Schulz E, Hink U, Wenzel P, Post F, Jabs A, Münzel T. Early outcome after implantation of Absorb bioresorbable drug-eluting scaffolds in patients with acute coronary syndromes. *EuroIntervention*. 2014;9:1036–1041. doi: 10.4244/EIJV9I9A176.

32. Kajiya T, Liang M, Sharma RK, Lee CH, Chan MY, Tay E, Chan KH, Tan HC, Low AF. Everolimus-eluting bioresorbable vascular scaffold (BVS) implantation in patients with ST-segment elevation myocardial infarction (STEMI). *EuroIntervention*. 2013;9:501–504. doi: 10.4244/EIJV9I4A80.

33. Capodanno D, Gori T, Nef H, Latib A, Mehilli J, Lesiak M, Caramanno G, Naber C, Di Mario C, Colombo A, Capranzano P, Wiebe J, Araszkiewicz A, Geraci S, Pyxaras S, Mattesini A, Naganuma T, Münzel T, Tamburino C. Percutaneous coronary intervention with everolimus-eluting bioresorbable vascular scaffolds in routine clinical practice: early and midterm outcomes from the European multicentre GHOST-EU registry. *EuroIntervention*. 2015;10:1144–1153. doi: 10.4244/EIJY14M07_11.

**SUPPLEMENTAL MATERIAL**

**Supplemental Methods**


Porcine ex vivo arterio-venous shunt model


Experimental set-up

Three consecutive stents were deployed in Sylgard mock vascular phantoms (1). The Sylgard conduits (ID 2.70 mm × 11 cm length) were fabricated using 316L stainless steel tubing and commercial elastomer kit (Sylgard®-184, Dow Corning). Stents were deployed to nominal diameter (3.0 mm) in room temperature serum prepared from the experimental animal. Before deploying stents, the tubing was mounted in a fixed apparatus. The extent of platelet aggregation at stent struts was studied after exposure to circulating blood for 1 hour in an established porcine arteriovenous carotid to jugular shunt model (2).


Target blood activated clotting times (ACT) between 150s and 200s were achieved with intravenous heparin (100 IU/kg) dosing without anti-platelet agents such as clopidogrel or aspirin. Two shunts were studied in each animal. Shunt positions were numerically noted as proximal, mid, and distal relative to the arterial side. Before establishing blood flow through the circuit, stents were primed with autologous platelet-poor plasma. During experiments, stented tubing was maintained in a 37°C water bath and flow rates were monitored continuously using an ultrasonic transducer (Transonic, Ithaca, NY). At the conclusion of each run, stents were gravity perfused with Ringer's Lactate, fixed in 10% neutral buffered formalin and bisected longitudinally. One stent half was immunostained using specific platelet markers (CD61/CD42b) relevant for aggregation of thrombocytes and examined *en*

*face* by confocal microscopy (CM) as well as scanning electron microscopy (SEM), while the other half was processes for inflammatory monocyte markers (CD14/PM-1) and examined *en face* by CM.

**Blood coagulation and platelet function**

Blood was serially drawn for coagulation and platelet function profiles pre-shunt (baseline) and after each experimental run to confirm the absence of coagulation and platelet function abnormalities. Indices of coagulation, platelet number and function included platelet count, prothrombin time, partial thromboplastin time, and light transmission aggregometry. In addition, pig platelet factor 4 release was also assessed in collected plasma using a commercial ELISA kit (Cat No. ab156530, Abcam, Cambridge, MA, sensitivity = 0.1ng/ml) according to manufacturer's instructions.

*Immunofluorescent Staining and confocal microscopy*

CD61 / CD42b

Stent halves were incubated overnight in 4°C in an antibody cocktail directed against specific platelet markers; CD61 as a marker of platelet aggregation (Immunotech, IM0540, dilution 1:100, Beckman Coulter, CA) and CD42b as a marker of platelet adhesion (Santa Cruz, sc-7070, dilution 1:40, Dallas, TX) to capture both originating and propagated platelet thrombus. Positive staining was visualized using a secondary antibody conjugated to an Alexa Fluor® 488 fluorophore. After immunostaining, nuclei were counterstained with DAPI (Invitrogen) and stents were mounted *'en face'* on glass slides and cover slipped in aqueous mounting media. The entire stent surface was scanned using predetermined "fixed"

parameters incorporating a tile feature with Z stack imaging (Zeiss, LSM 700, Zen 2011 software). The positive area of platelet staining was analyzed by proprietary software (*Zen image analysis tool)* within defined regions of interest, which were maintained for all examined samples (40 mm$^2$) and reported as absolute positive area (mm$^2$) and percent positive area (%) which was calculated by dividing the absolute positive area by the entire stented area within the bisected segment of the artery. In addition, the relative percentage of positive staining was also calculated by dividing the absolute positive area by total stent surface area.

CD14 / PM-1

Four stent halves from each group were exposed overnight at 4°C to anti-CD14 antibody (Novus Biological, NB100-77758, dilution 1:40) for monocyte staining or anti-PM1 (BMA Biological, T3503, dilution 1:800) for neutrophil staining.  The antibody reaction was visualized with an Alexa Fluor 488 donkey anti-mouse secondary antibody (Invitrogen, Carlsbad, CA dilution 1:150) for anti-CD14 and an Alexa Fluor 555 donkey anti-mouse secondary antibody (Invitrogen, Carlsbad, CA dilution 1:150) for anti-PM1. DAPI (Invitrogen) was used as the nuclear counter-stain. The specimens were then mounted "en face" on glass slides, cover slipped using aqueous mounting media, and three representative images were acquired by Zeiss LSM 700 laser confocal microscope at 20x magnification with Z-stack. The number of inflammatory cells was counted in randomly selected areas of stent struts remaining free of platelet thrombus.

*Scanning electron microscopy (SEM)*

The remaining stent halves were processed for SEM. Specimens were dehydrated, critically

point dried, and sputter-coated with gold. Digital images were acquired using a Hitachi Model 3600N (Hitachi High-Technologies Science America, Inc., Northridge, CA). Low power (15 x magnifications) images of the entire luminal surface were collected to assess the extent of thrombus attached to the strut surfaces. Stitched low power montage images of the entire luminal surface were then assembled into a single image using proprietary software. Higher power photographs of regions of interest were also taken at incremental magnifications of (50x, 200x, 600x, and 2000x). From these images, percent endothelial coverage between and above stent struts was semi-quantified by visual estimation from the proximal to distal end. The percentage endothelialization was recorded for the areas above and between struts. Endothelial cells were identified as sheets of spindle or polygonal shaped monolayers in close apposition, a distinguishing feature from other cell types in en face preparations.

*Rabbit Model of Iliac Stent Implantation*

Experimental set-up

*Balloon Endothelial Denudation*

Before deploying implants, both iliofemoral arteries underwent an endothelial denudation procedure as described previously. A 3.0 × 8 mm standard angioplasty balloon catheter (Voyager, Abbott Vascular) was placed in the distal iliofemoral artery over a guide wire using fluoroscopic guidance and inflated to 7 ATM with 50/50 contrast/saline. The balloon catheter was then withdrawn proximally (retrograde) in its distended state to the level of the iliac bifurcation involving a distance of approximately 2 cm. The balloon was then deflated and repositioned in the distal iliac artery to the original location. A second pullback was repeated with the existing balloon now inflated to 9 ATM. Using the same balloon catheter, the

denuding procedure was performed on the contralateral iliac artery. At the conclusion of the procedure, the dilation catheter was deflated and removed.

*Stent Implantation*

Immediately following bilateral iliac artery balloon denudation, devices were deployed in the denuded section of iliofemoral arteries. The pre-mounted stent-catheter (3.0 x 18 mm) was delivered into each iliac artery using a guide wire under fluoroscopic guidance. In the target area the stent was implanted at nominal inflation pressure. Following stent deployment, angiography was repeated to document vessel patency.

*Immunofluorescent Staining*

The stented artery halves designated for CM were subsequently stained overnight at 2 to 8°C for CD31/PECAM-1 (Dako, Carpenteria, CA, dilution 1:20) or RAM-11 (Dako, Carpenteria, CA, dilution 1: 400), respectively, after rinsing. The antibody reaction was visualized with an Alexa Fluor 488 donkey anti-mouse secondary antibody (Invitrogen, Carlsbad, CA dilution 1:150) for CD31/PECAM-1 and with an Alexa Fluor 555 donkey anti-mouse secondary antibody (Invitrogen, Carlsbad, CA dilution 1:150) for RAM-11. DAPI (Invitrogen, Carlsbad) was used as the nuclear counter-stain.

Image analysis

*(1) CD31/PECAM Immunofluorescent Staining*

The percentage of endothelial surface coverage based on immunostaining against CD31/PECAM-1 above and between struts was estimated visually from each strut area on 5x magnification of en face images. Proximal segments adjacent to the stent served as a

positive control for immunostaining.  For illustration, confocal z-stack images with tile imaging were acquired at 5x magnification. Representative high power fluorescent images of the luminal surface from (proximal, middle, and distal) regions of the stent were also acquired by CM using a $\times$20 objective with optical Z-stack acquisition to document the extent of CD31 expression staining of endothelial junctions. Semi-quantification of CD31/PECAM-1 positive endothelial cells was achieved by visual assessment above and between stent struts and expressed as median with lower (25th percentile) and upper quartiles (75th percentile).

*(2) RAM-11 Immunofluorescent Staining*

RAM-11 expression was semi-quantified within a region of interest that included the entire stented segment and was kept constant for all analyzed specimens ($30mm^2$). RAM-11 positive staining was assessed using ZEN image analysis tool (Zeiss ZEN black edition 2011, Carl-Zeiss Microscopy, Jena, Germany), which was used to measure the  fluorescent-positive area within the previously defined region of interest. Representative high power fluorescent images of the luminal surface from (proximal, middle, and distal) regions of the stent were also acquired by CM using a 20x objective with optical Z-stack acquisition to document the extent of RAM-11 expression.

Supplemental Table 1

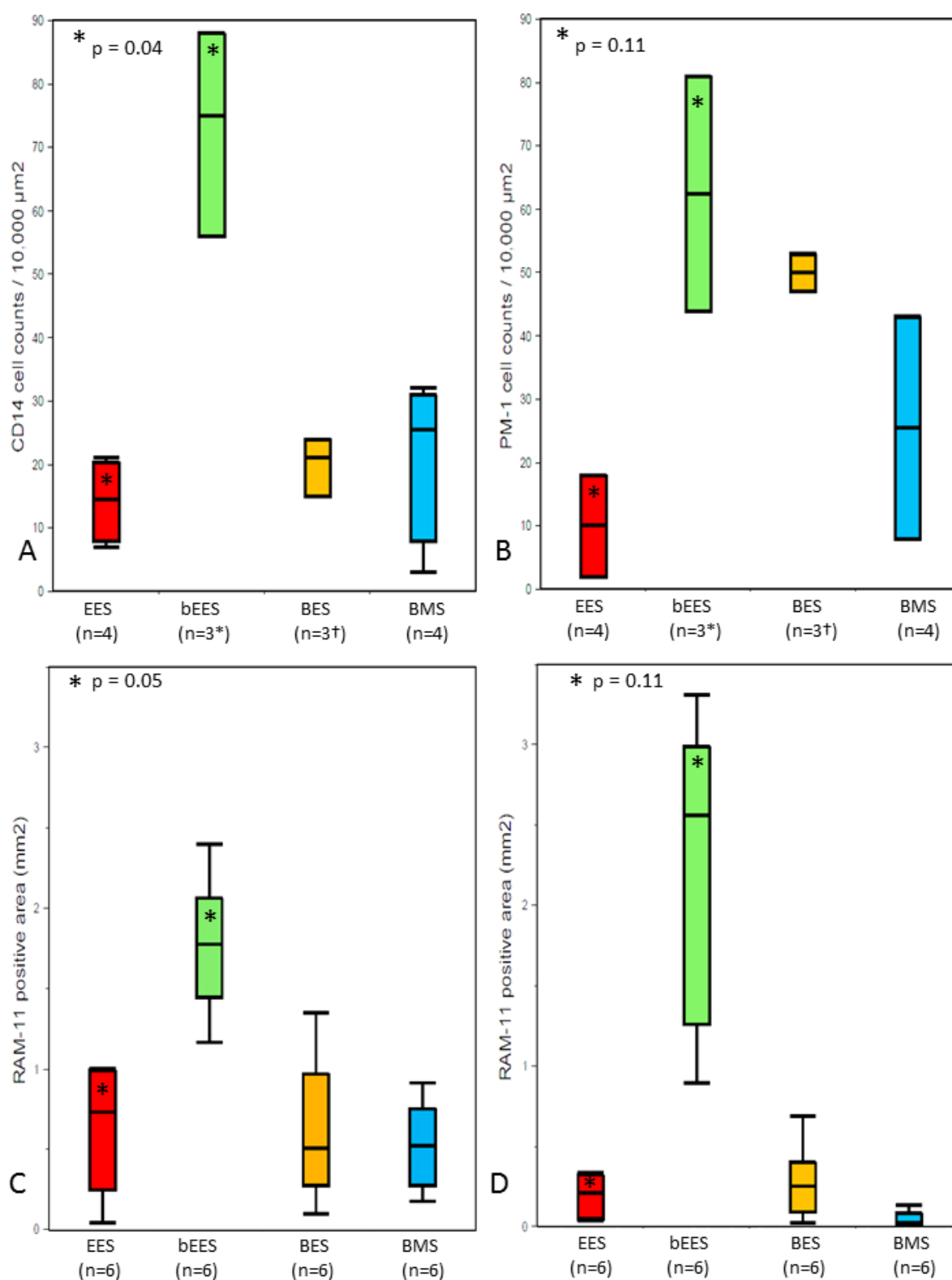| | | Inflammatory marker | | Median | Percentile 25th | Percentile 75th | P value |
|---|---|---|---|---|---|---|---|
| Ex-vivo AV shunt model | CD14 Positive Cells / 10,000 µm² | Biodegradable polymer metallic everolimus eluting stent (EES) | n = 4 | 14.5 | 8 | 20.3 | |
| | | Fully bioabsorbable everolimus eluting stent (bEES) | n = 3* | 75 | 56 | 88 | EES vs. bEES p = 0.04 |
| | | Biodegradable polymer metallic biolimus eluting stents (BES) | n = 3† | 21 | 15 | 24 | EES vs. BES p = 1.00 |
| | | Bare metal stents (BMS) | n = 4 | 25.5 | 8 | 31 | EES vs. BMS p = 1.00 |
| | PM1 Positive Cells / 10,000 µm² | Biodegradable polymer metallic everolimus eluting stent (EES) | n = 2 | 10 | 2 | 18 | |
| | | Fully bioabsorbable everolimus eluting stent (bEES) | n = 2 | 62.5 | 44 | 81 | EES vs. bEES p = 0.11 |
| | | Biodegradable polymer metallic biolimus eluting stents (BES) | n = 2 | 50 | 47 | 53 | EES vs. BES p = 0.29 |
| | | Bare metal stents (BMS) | n = 2 | 25.5 | 8 | 43 | EES vs. BMS p = 0.84 |
| Rabbit stent implantation model | 14 days — RAM-11 Positive Area (mm²) | Biodegradable polymer metallic everolimus eluting stent (EES) | n = 6 | 0.7 | 0.3 | 1.0 | |
| | | Fully bioabsorbable everolimus eluting stent (bEES) | n = 6 | 1.8 | 1.4 | 2.1 | EES vs. bEES p = 0.05 |
| | | Biodegradable polymer metallic biolimus eluting stents (BES) | n = 6 | 0.5 | 0.3 | 1.0 | EES vs. BES p = 1.00 |
| | | Bare metal stents (BMS) | n = 6 | 0.5 | 0.3 | 0.7 | EES vs. BMS p = 1.00 |
| | 28 days — RAM-11 Positive Area (mm²) | Biodegradable polymer metallic everolimus eluting stent (EES) | n = 6 | 0.2 | 0.1 | 0.3 | |
| | | Fully bioabsorbable everolimus eluting stent (bEES) | n = 6 | 2.6 | 1.3 | 3.0 | EES vs. bEES p = 0.11 |
| | | Biodegradable polymer metallic biolimus eluting stents (BES) | n = 6 | 0.3 | 0.1 | 0.4 | EES vs. BES p = 1.00 |
| | | Bare metal stents (BMS) | n = 6 | 0.1 | 0.1 | 0.4 | EES vs. BMS p = 0.61 |

**Supplemental Table 1.** Inflammatory markers in the porcine ex-vivo arteriovenous shunt model based on fluorescent staining against monocyte marker CD14, neutrophil marker PM-1 and macrophage adhesion after 14 and 28 days assessed by RAM-11 expression in the rabbit stent implantation model. Values represent median with lower (25th percentile) and upper quartiles (75th percentile). No assessment of inflammatory reaction could be performed in one *bEES and one †BES due to extensive thrombus formation which obscured inflammatory cells adhering to the stent surface. EES denotes biodegradable polymer metallic everolimus eluting stent. bEES denotes fully bioabsorbable everolimus eluting stent. BES denotes biodegradable polymer metallic biolimus eluting stent. BMS denotes bare metal stent.

Supplemental Table 2

| Endothelial Coverage by CD31 / PECAM-1 | | | Median | Percentile 25th | Percentile 75th | P value |
|---|---|---|---|---|---|---|
| **14 days** | **Above Struts (%)** | Biodegradable polymer metallic everolimus eluting stent (EES) | n = 6 | 1.6 | 0 | 3.7 | |
| | | Fully bioabsorbable everolimus eluting stent (bEES) | n = 6 | 0 | 0 | 0 | EES vs. bEES p = 0.55 |
| | | Biodegradable polymer metallic biolimus eluting stents (BES) | n = 6 | 0.4 | 0 | 2.0 | EES vs. BES p = 1.00 |
| | | Bare metal stents (BMS) | n = 5* | 65.4 | 45.2 | 74.8 | EES vs. BMS p = 0.15 |
| | **Between Struts (%)** | Biodegradable polymer metallic everolimus eluting stent (EES) | n = 6 | 6.1 | 1.3 | 14.8 | |
| | | Fully bioabsorbable everolimus eluting stent (bEES) | n = 6 | 3.6 | 1.8 | 4.8 | EES vs. bEES p = 1.00 |
| | | Biodegradable polymer metallic biolimus eluting stents (BES) | n = 6 | 8.7 | 5.5 | 11.3 | EES vs. BES p = 1.00 |
| | | Bare metal stents (BMS) | n = 5* | 71.1 | 50.4 | 78.3 | EES vs. BMS p = 0.05 |
| **28 days** | **Above Struts (%)** | Biodegradable polymer metallic everolimus eluting stent (EES) | n = 6 | 11.8 | 4.4 | 22.1 | |
| | | Fully bioabsorbable everolimus eluting stent (bEES) | n = 6 | 1.1 | 0 | 3.5 | EES vs. bEES p = 0.20 |
| | | Biodegradable polymer metallic biolimus eluting stents (BES) | n = 6 | 14.6 | 4.2 | 21.3 | EES vs. BES p = 1.00 |
| | | Bare metal stents (BMS) | n = 6 | 83.0 | 43.8 | 100 | EES vs. BMS p = 0.23 |
| | **Between Struts (%)** | Biodegradable polymer metallic everolimus eluting stent (EES) | n = 6 | 17.3 | 7.4 | 32.1 | |
| | | Fully bioabsorbable everolimus eluting stent (bEES) | n = 6 | 4.1 | 2.6 | 7.5 | EES vs. bEES p = 0.33 |
| | | Biodegradable polymer metallic biolimus eluting stents (BES) | n = 6 | 18.4 | 10.9 | 32.0 | EES vs. BES p = 1.00 |
| | | Bare metal stents (BMS) | n = 6 | 83.9 | 46.6 | 100 | EES vs. BMS p = 0.20 |

**Supplemental Table 2.** Rabbit stent implantation model. Endothelial coverage above and between stent struts semi-quantified from CD31/PECAM-1 immunostaining by visual assessment after 14 and 28 days.  Values represent median with lower (25th percentile) and upper quartiles (75th percentile). (* One BMS was excluded because of artificial disruption of the endothelial layer). EES denotes biodegradable polymer metallic everolimus eluting stent. bEES denotes fully bioabsorbable  everolimus eluting stent. BES denotes biodegradable polymer metallic biolimus eluting stent. BMS denotes bare metal stent.

Supplemental Figure 1

**Supplemental Figure 1.** Inflammatory markers in the ex-vivo arteriovenous shunt model **(A,B)** and the rabbit stent implantation model **(C,D)**. Box and whisker diagrams represent median with lower (25th percentile) and upper quartiles (75th percentile) and whiskers for minimum and maximum value. EES denotes biodegradable polymer metallic everolimus eluting stent. bEES denotes fully bioabsorbable everolimus eluting stent. BES denotes biodegradable polymer metallic biolimus eluting stent. BMS denotes bare metal stent.

**(A)** Acute Monocyte adhesion based on CD14 positive cell counts using confocal microscopy analysis in the ex-vivo arteriovenous shunt model. EES and BMS consisted of n=4 stents per group, while one *bEES stent and one †BES stent was excluded from the analysis due to extensive thrombus formation which obscured inflammatory cells adhering to the stent surface.

**(B)** Neutrophil cell adhesion based on PM-1 positive cell counts using confocal microscopy analysis in the ex-vivo arteriovenous shunt model. EES and BMS consisted of n=4 stents per group, while one *bEES stent and one †BES was excluded from the analysis due to extensive thrombus formation which obscured inflammatory cells adhering to the stent surface.

**(C, D)** Macrophage adhesion based on confocal microscopy analysis of RAM-11 expression at 14 days (C) and 28 days (D) after device implantation. EES, bEES, BES and BMS consisted of n=6 in each group.

**Supplemental references**

1. Colombo A, Zahedmanesh H, Toner DM, Cahill PA, Lally C. A method to develop mock arteries suitable for cell seeding and in-vitro cell culture experiments. Journal of the mechanical behavior of biomedical materials 2010;3:470-7.

2. Chin-Quee SL, Hsu SH, Nguyen-Ehrenreich KL et al. Endothelial cell recovery, acute thrombogenicity, and monocyte adhesion and activation on fluorinated copolymer and phosphorylcholine polymer stent coatings. Biomaterials 2010;31:648-57.

# Circulation
## Cardiovascular Interventions

American Heart Association®

Thrombogenicity and Early Vascular Healing Response in Metallic Biodegradable
Polymer-Based and Fully Bioabsorbable Drug-Eluting Stents
Tobias Koppara, Qi Cheng, Kazuyuki Yahagi, Hiroyoshi Mori, Oscar David Sanchez, Julia
Feygin, Eric Wittchow, Frank D. Kolodgie, Renu Virmani and Michael Joner

The online version of this article, along with updated information and services, is located on the
World Wide Web at:
http://circinterventions.ahajournals.org/content/8/6/e002427

Data Supplement (unedited) at:
http://circinterventions.ahajournals.org/content/suppl/2015/05/29/CIRCINTERVENTIONS.115.002427.DC1.html